IEEE Access
Multidisciplinary | Rapid Review | Open Access Journal

Received December 10, 2018, accepted January 1, 2019, date of publication January 14, 2019, date of current version April 1, 2019.

Digital Object Identifier 10.1109/ACCESS.2019.2892648

Novel Land Cover Change Detection Method Based on k-Means Clustering and Adaptive Majority Voting Using Bitemporal Remote Sensing Images

ZHIYONG LV[1,2], TONGFEI LIU[1], CHENG SHI[1], JÓN ATLI BENEDIKTSSON[3], (Fellow, IEEE), AND HEJUAN DU[4]

[1]School of Computer Science and Engineering, Xi'an University of Technology, Xi'an 710048, China
[2]Key Laboratory of Spatial Data Mining and Information Sharing of Ministry of Education, National Engineering Research Centre of Geospatial Information Technology, Fuzhou University, Fuzhou 350116, China
[3]Faculty of Electrical and Computer Engineering, University of Iceland, IS 107 Reykjavik, Iceland
[4]School of Information Engineering, Tibet Nationality University, Xianyang 712089, China

Corresponding author: Zhiyong Lv (lvzhiyong_fly@hotmail.com)

This work was supported in part by the Key Laboratory of Spatial Data Mining and Information Sharing of Ministry of Education, Fuzhou University, under Grant 2019LSDMIS01, in part by the Nature Science National Foundation of China under Grant 61701396, and in part by the Natural Science Foundation of Shaanxi Province under Grant 2017JQ4006.

ABSTRACT Land cover change detection (LCCD) based on bitemporal remote sensing images has become a popular topic in the field of remote sensing. Despite numerous methods promoted in recent decades, an improvement on the usability and performance of these methods has remained necessary. In this paper, a novel LCCD approach based on the integration of k-means clustering and adaptive majority voting (k-means_AMV) techniques have been developed. The proposed k-means_AMV method consists of three major techniques. First, to utilize the contextual information in an adaptive manner, an adaptive region around a central pixel is constructed by detecting the spectral similarity between the central pixel and its eight neighboring pixels. Second, when the extension for the adaptive region is terminated, the k-means clustering method is applied to determine the label of each pixel within the adaptive region. Finally, an existing AMV technique is used to refine the label of the central pixel of the adaptive region. When change magnitude image (CMI) is scanned and processed in this manner, the label of each pixel in the CMI can be refined and the binary change detection map can be generated. Three image scenes related to different land cover change events are adapted to test the effectiveness and performance of the proposed k-means_AMV approach. The results show that the proposed k-means_AMV approach demonstrates better detection accuracies and visual performance than that of the several extensively used methods.

INDEX TERMS Adaptive majority voting, k-means clustering, land cover change detection, remote sensing images.

I. INTRODUCTION

Land cover change detection (LCCD) using bitemporal remote sensing images has been a popular topic in remote sensing application [1]–[3] because LCCD can provide timely and large-scale land cover change information for assisting urban development plans, such as urban expansion [4], [5], urban build-up changing [6], [7], and city surface temperature change analysis [8]. In addition, LCCD also plays an important role in the Earth's surface resource monitoring, including landslide inventory mapping [9]–[11], forest monitoring [12]–[14], and environmental evaluation [15]–[17].

Numerous change detection techniques have been promoted and applied in practice [18]–[23]. Considering their detection results, these methods can be categorized into

The associate editor coordinating the review of this manuscript and approving it for publication was Weimin Huang.

''post-classification change detection method'' and ''binary change detection method'' [3], [24]. We concentrate on the binary change detection method because it is straightforward and operational [3]; we also review its related methods as follows. The binary change detection method has two major steps, namely, generating of change magnitude image (CMI) and binary threshold to divide the CMI into binary change detection maps (BCDM). The most popular methods for generating a CMI are image difference [22], [25], image ratios [24], and change vector analysis [26], [27]. Furthermore, several notable derived methods for generating CMI have drawn attention; for example, Chen *et al.* [28] proposed a spectral gradient difference for measuring the change magnitude between bitemporal multi-spectral remote sensing images; moreover, Lv and Zhang [20] promoted a change magnitude for very high resolution (VHR) remote sensing images on the basis of adaptive contextual information. In addition to generating a binary detection map, a binary threshold is required to obtain the final change inventory map. The most frequently used binary threshold-determining methods are Otsu's method [20], [29] and expectation maximization [30]. However, an optimal binary threshold for balancing pseudo-changes and an unchanged area is difficult to obtain given the uncertainty and complexity of a changed area in terms of change magnitude and spatial distribution. According to several studies, determining an optimal binary threshold in practical application for LCCD is time-consuming [21], [22], [31].

In the past decades, various LCCD methods have been promoted and applied in practice [1], [17], [32]–[34]. For example, Lunetta *et al.* [33] explored the use of 250 m multi-temporal MODIS NDVI 1-day composite data to provide an automated change detection; similar change detection cases based on the MODIS data can be found in [35]–[37]. In addition, Landsat satellite images are another popular data source for LCCD, such as the related cases studied in [38]–[40]. Furthermore, the data acquired by the Sentinel satellite are frequently used for detecting land cover change [41]–[43]. With the development of remote sensing techniques [44], [47], LCCD based on the remote sensing images with high or VHR has drawn attention. For example, Bruzzone and Bovolo [46] promoted a novel framework for VHR multispectral image LCCD; Du *et al.* [47] developed a radiometric normalization method for improving the quality of LCCD for VHR remote sensing satellite images; Bynn *et al.* [48] extracted a flood area using the bitemporal VHR remote sensing images. In addition to the aforementioned pixel-based LCCD methods for VHR remote sensing images, object-based LCCD approaches are popular for LCCD using VHR remote sensing images [49]–[51]. Although these approaches have been promoted and applied in practice, the following limitations must be noted: (1) given that the variance is relatively higher in intra-class for VHR image than in the median-low spatial resolution images, a fine resolution does not mean higher detection accuracies; (2) typically, the performance of object-based methods depends considerably on the performance of segmentation; however, parameters of multiscale segmentation depend on data and experience; and (3) few methods are general for median-low spatial resolution and VHR remote sensing images; this situation may result in difficulty in selecting a method for a practitioner with inadequate experience.

In recent years, numerous methods have been proposed for LCCD using very high spatial resolution remote sensing images. For example, Zhang *et al.* [52] proposed a level set evolution with local uncertainty constraints (LSELUC) unsupervised LCCD method and applied the technique for Landsat and SPOT-5 remote images with resolutions of 30 and 2.5 m/pixel, respectively; Bazi *et al.* [53] suggested unsupervised LCCD methods on the basis of multispectral remote sensing image with a level set method (MLS), and Celik [25] provided an unsupervised LCCD method using principal component analysis and K-means clustering (PCA_Kmeans). In addition, K-means has been used successfully in image segmentation [56]. An observational superiority of this unsupervised LCCD approach exists because it is unsupervised and has no requirement of the binary threshold. However, detection accuracies, performance, and usability must still be improved.

In this study, a simple yet effective change detection method with high generality is proposed by integrating K-means clustering with a majority voting approach using an adaptive region. An adaptive region around a pixel in the CMI is initially generated on the basis of two pre-defined constraints [20]. Then, the label of each pixel within the extended region is determined by the K-means clustering algorithm. Finally, the label of the central pixel is refined by an adaptive majority voting (AMV) strategy [54]. When each pixel of the entire CMI is scanned and refined in this manner, a BCDM depicts the size, and the spatial distribution of land cover change will be acquired.

The remainder of this paper is organized as follows. In Section II, the proposed K-means_AMV is introduced. In Section III, experiments based on three bitemporal images are compared. In Sections IV and V, discussion and conclusion are presented, correspondingly.

II. PROPOSED k-MEANS CLUSTERING INTEGRATING AMV TECHNIQUE (K-MEANS_AMV)

The proposed K-means_AMV approach has the following principal steps, as illustrated in Fig. 1. First, for the bitemporal images, the CMI is generated using the image difference approach. Furthermore, the specific training samples for changed and unchanged are prepared manually on the basis of the CMI. In addition, a pixel is used as the ''central-pixel,'' and an adaptive region is extended gradually around the central pixel using two pre-defined parameters. Second, the pixels within the extended region is labeled through the K-means approach on the basis of the training samples. Finally, the label of the central pixel is refined by the AMV approach. The entire CMI is processed and refined pixel-by-pixel, whereas the BCDM based on bitemporal remote

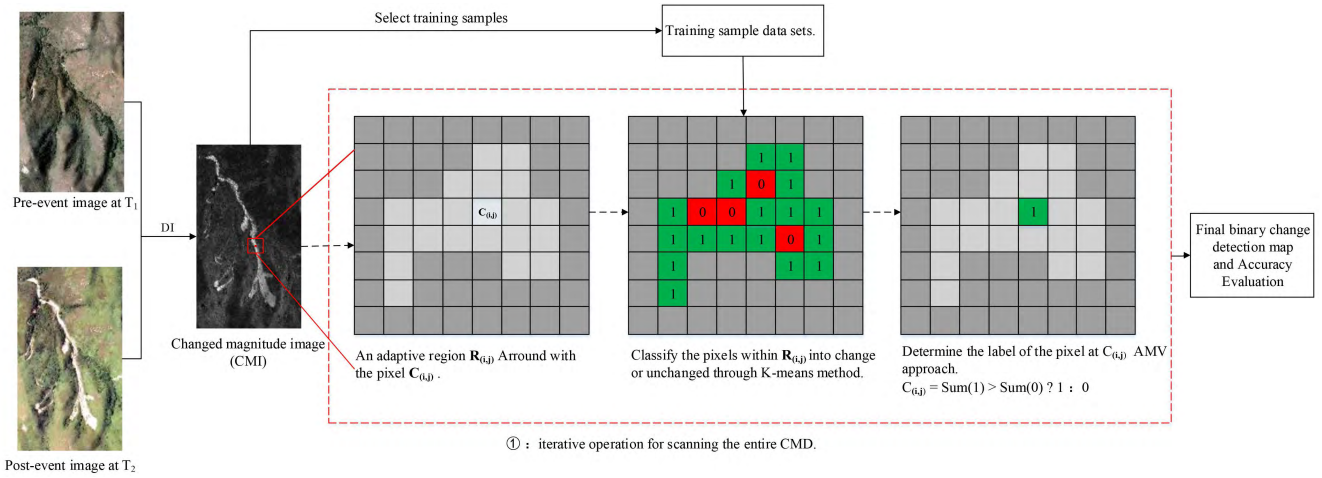

FIGURE 1. Flowchart of the proposed approach.

sensing images are available. Further details will be presented in the subsequent sections.

A. GENERATING AN ADAPTIVE REGION AROUND A CENTRAL PIXEL

Certain literature has demonstrated that utilizing the spatial information of remote sensing images in an adaptive manner gains an advantage in smoothing noise and preserving the details of ground targets [55], [57], [58] because, according to Tobler's first law of geography, everything is related to everything else, and things that are close are more related than the things that are distant [59]. Remote sensing image depicts the earth surface of a geographical area; thus, pixels with a significant proximity tend to belong to the same object, and the arrangement of pixels in a spatial domain typically relates to the shape and size of a ground object in the remote sensing image. However, the shape and size of various ground objects are different. Therefore, in our proposed approach, an adaptive region is used to describe the spatial feature accurately and obtain a high detection accuracy.

In the proposed K-means_AMV approach, constructing an adaptive region plays a pivotal role. Here, we briefly review the adaptive extension techniques as follows: For a given CMI image, $1 < i < W$, $1 < j < H$, where W and H are the width and height of the CMI, respectively. Under this context, one pixel $C(i, j)$ is taken as the "central-pixel" for an extension. The extension around the pixel $C(i, j)$ is a recursive progress, and the extension will be performed while the following conditions are satisfied: (1) the spectral similarity between the pixel $C(i, j)$ and its eight-connected neighboring pixels is less than the predefined parameter T_1, and (2) the total number of the pixels within the extended adaptive region is not greater than another predefined parameter T_2. An adaptive region around a pixel will be gradually extended pixel-by-pixel; the recursive extension will be terminated when either of the two conditions is unsatisfied. Here, the extended adaptive region around the pixel $C(i, j)$ is assigned as R_{ij}. Additional details on the adaptive extension technique can be tracked [55].

B. LABELING EACH PIXEL THROUGH k-MEANS CLUSTERING ALGORITHM

K-means is adopted here for acquiring the label of each pixel within an adaptive region R_{ij}. Therefore, we briefly review the K-means algorithm in this section. The K-means algorithm is a conventional clustering algorithm for unsupervised learning; this algorithm aims to divide observations into K-clusters in which each observation belongs to the cluster with the nearest mean, thus serving as a prototype of the cluster. This algorithm has been applied to the LCCD and classification on the basis of remote sensing images; for example, Celik [25] proposed an unsupervised change detection method using PCA and K-means; Lv *et al.* [60] used a density-based K-means clustering algorithm to select a training sample for remote sensing classification.

For the binary change detection problem, a set of observational pixels that are within the adaptive region R_{ij} is classified through the K-means clustering algorithm. Therefore, k is equal to 2; that is, the pixels will be classified in the CMI into two categories, namely, changed and unchanged. In addition, for the K-means algorithm, another important issue is to select cluster centers for the changed and unchanged areas. To solve this problem, the training samples for the changed and unchanged areas are manually selected from the CMI. Here, the set of training sample for the changed area is defined as S_1, and the unchanged area sample set is defined as S_0. Under this context, the clustering center can be expressed using Formulas 1 and 2. Where L_{ij} is the label of the pixel p_{ij}, and "0" and "1" indicate the "unchanged" and "changed" categories, respectively. The label of the pixel within an extended region is determined by the distance between the pixel and the clustering center; a high probability of the pixel belongs to the clustering center when the distance is near a clustering center. The pixels within the R_{ij} are scanned and

labeled pixel-by-pixel to obtain the label of all pixels in R_{ij}.

$$C_1 = \frac{1}{N} \cdot \sum_{n=1}^{n=N} p_n^c, \tag{1}$$

$$C_0 = \frac{1}{M} \cdot \sum_{n=1}^{n=M} p_n^{uc}, \tag{2}$$

where C_1 and C_0 are the changed and unchanged clustering centers, correspondingly; p_n^c and p_n^{uc} are the spectral values of a pixel within the S_1 and S_0, respectively; and N and M denote the total number of the pixels within S_1 and S_0, correspondingly. Then, the distance between each pixel p_{ij}, which is within the R_{ij} and the two clustering centers, is measured using Formulas 3 and 4, respectively.

$$d_{ij}^{C_1} = \left\| p_{ij} - C_1 \right\|, \tag{3}$$

$$d_{ij}^{C_0} = \left\| p_{ij} - C_0 \right\|, \tag{4}$$

where $d_{ij}^{C_1}$ and $d_{ij}^{C_0}$ denote the distance between the pixel p_{ij} and the clustering center C_1 and C_0, correspondingly. Therefore, the label of p_{ij} is determined by Formula 5.

$$L_{ij} = \begin{cases} 1, & d_{ij}^{C_1} < d_{ij}^{C_0} \\ L_{ij}, & d_{ij}^{C_1} = d_{ij}^{C_0} \\ 0, & d_{ij}^{C_1} \geq d_{ij}^{C_0}, \end{cases} \tag{5}$$

C. REFINING THE LABEL OF THE CENTRAL-PIXEL FOR AN ADAPTIVE EXTENDED REGION

Although each label of the pixels within an adaptive region is defined relatively in the previous section, refining the label of the central pixel accurately is necessary. Therefore, an AMV algorithm, which has been investigated in [55], is used here. The AMV algorithm has been applied to refine and enhance the performance of LCCD and classification, similar to the works of Lv *et al.* [61], who proposed an object-based majority voting method to refine the raw LCCD, and Cui *et al.* [54], who used a dual-AMV strategy to refine classification maps.

In Section II-A, the pixel $C(i, j)$ is used as the "central-pixel" for an extension region, and the extended adaptive region around the pixel $C(i, j)$ is assigned as R_{ij}. To further improve the performance of the central-pixel $C(i, j)$ that is labeled by the K-means clustering algorithm, the label of the central pixel is refined using the AMV algorithm. On the basis of the AMV algorithm, the final label of the seed-pixel $C(i, j)$ can be determined by Formula 6. Where $L_{C(i,j)}$ is the final label of the central-pixel $C(i, j)$ that is refined by the AMV algorithm, and "1" and "0" express the "changed" and "unchanged," correspondingly; $P_{ij}^c(R_{ij})$ and $P_{ij}^{uc}(R_{ij})$ are the total number of changed and unchanged pixels within an adaptive extended region for the CMI, respectively. The final label of the central-pixel is determined by comparing the total number of changed and unchanged pixels within an adaptive extended region. Each pixel in the CMI will be scanned and calculated in this manner to generate the final BCDM.

$$L_{C(i,j)} = \begin{cases} 1, P_{ij}^c(R_{ij}) > P_{ij}^{uc}(R_{ij}) \\ L_{i,j}, P_{ij}^c(R_{ij}) = P_{ij}^{uc}(R_{ij}) \\ 0, P_{ij}^c(R_{ij}) < P_{ij}^{uc}(R_{ij}), \end{cases} \tag{6}$$

III. EXPERIMENT

In this section, three land cover change events depicted by bitemporal remote sensing images are used to evaluate the effectiveness of the proposed K-means_AMV approach. First, the image data for each event are described in detail. Second, the optimal parameter of each approach is estimated. Finally, the visual performance and quantitative evaluation of the LCCD maps are shown for comparisons with other extensively used methods [25], [52], [53].

A. DATASET DESCRIPTION

In Fig. 2, the first image datasets depict a landslide in Lantau Island, Hong Kong, China. These image datasets are captured using Zeiss RMK Top-1 aerial survey camera from the flying height of approximately 2400 m in April 2007 and July 2014. The size of These pair images is 923 × 593 pixels with a spatial resolution of 0.5 m/pixel. This area is covered with different land-use types, including trees, shrubs, gravel, and bare soil, as demonstrated in the bitemporal images in Fig. 2. In addition, the radiation in the bitemporal images varies in spectra because they are acquired at different times. The difference in land cover types and spectral radiation has become a challenge in detecting the landslide inventory map. Fig. 2-c exhibits a ground reference map, which is interpreted manually.

To further verify the efficiency of the proposed approach, other VHR remote sensing images are adopted in the second experiment. In Fig. 3, these images are captured by QuickBird satellite in June 2007 and November 2009, and the paired images cover an area of 950 × 1250 pixels with a spatial resolution of 0.61 m/pixel. Based on the scene of the bitemporal remote sensing images, the two image scenes vary in land cover types; the pre-event image is covered by most part of vegetation, and the post-event image is covered by buildings, roads, and farmlands. Variation in spectral value is observed because the pair images vary with season, although no changes occur. The detection of land cover change through the VHR remote sensing images remains a challenging task.

The third dataset is an open-access data, which are freely available for LCCD. The pair images are composed of two 8-bit images captured by Landsat-5 satellite on September 1995 and July 1996. The size of the image is 412 × 300 pixels with a spatial resolution of 30 m/pixel. This dataset depicts the water level change in a lake in Sardinia Island (Italy) using two remote sensing images captured at different times. The ground reference map is interpreted manually for experimental quantitative evaluation, as presented in Fig. 4-c.

As mentioned previously, three image datasets selected in our experiments vary in spatial resolution, data-sourcing, and

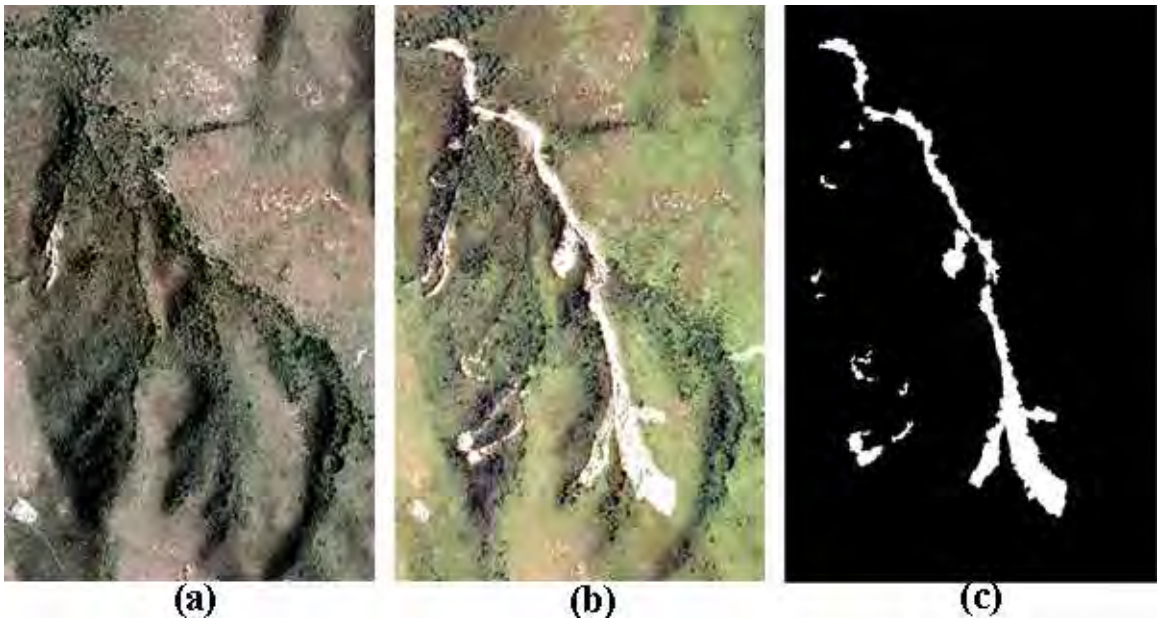

FIGURE 2. Landslide event in Lantau Island, Hong Kong, China: (a) pre-event image acquired April 2007; (b) post-event image acquired at July 2014; (c) ground reference map.

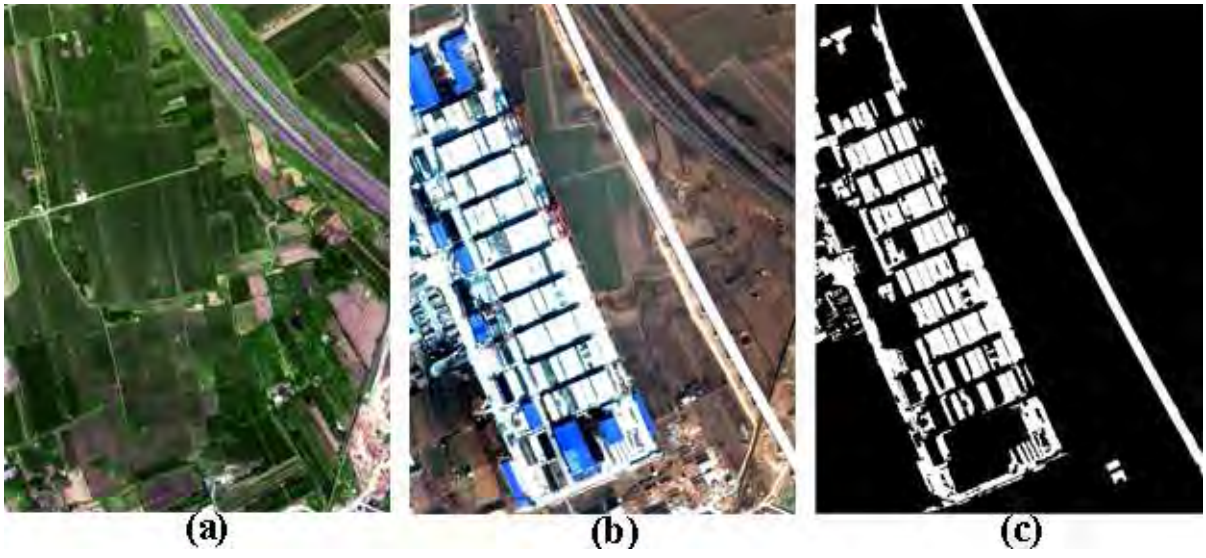

FIGURE 3. Land use change event in Ji Nan City, Shan Dong Province, China: (a) pre-event image acquired at June 2007; (b) post-event image acquired at November 2009; (c) ground reference map.

land cover change event. This data selection aims to verify the generality and robustness of the proposed approach. The details of the evaluation based on the three datasets are discussed as follows.

B. EXPERIMENTAL SETUP AND PARAMETER SETTING

To test the effectiveness of the proposed K-means_AMV approach for detecting land cover change using bitemporal remote sensing images, three widely used methods, namely, PCA-Kmeans [25], LSELUC [52], and MLS [53], are compared with the proposed K-means_AMV approach. For each dataset and method, the optimal parameters of each experiment are obtained through a trial-and-error approach; details of the parameter setting for each approach are summarized in Table 1. For the proposed K-means_AMV approach, to test the usability of the proposed approach, image difference and adaptive region mean distance (ARMD) [62], which has been used for LCCD, are adopted to generate the CMI of each image dataset. The proposed approaches coupled with the different generations of CMI, namely, the proposed-Diff and proposed-ARMD, are displayed in Table 1. In addition,

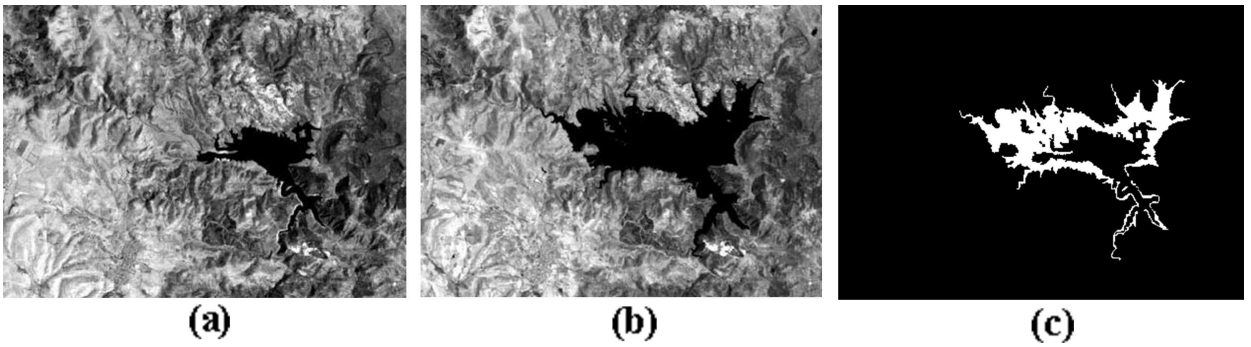

FIGURE 4. Sardinia Island area in Italy: (a) pre-event image acquired at September 1995; (b) post-event image acquired at July 1996; (c) ground reference map.

TABLE 1. Parameter settings of the different LCCD methods for each dataset.

Method	Parameter Settings		
	Hong Kong	Ji Nan	Sardinia
LSELUC [52]	$S = 9$	$S = 3$	$S = 3$
MLS [53]	$L = 4, \mu = 0.3$	$L = 2, \mu = 0.1$	$L = 2, \mu = 0.1$
PCA_Kmeans [25]	$h = 9, s = 3$	$h = 3, s = 3$	$h = 9, s = 5$
The proposed-Diff	$T_1 = 145, T_2 = 100$	$T_1 = 105, T_2 = 100$	$T_1 = 70, T_2 = 100$
The proposed-ARMD	$T_1 = 125, T_2 = 100$	$T_1 = 120, T_2 = 100$	$T_1 = 65, T_2 = 100$

the details of ground reference maps for each dataset are summarized in Table 2.

TABLE 2. Details of the ground reference map for each dataset.

Data Set	Number of Pixels in the Ground Reference for Each Dataset	
	No. of Unchanged Pixels	No. of Changed Pixels
Hong Kong	520746	26593
Ji Nan	987017	200483
Sardinia	115974	7626

C. VISUAL IDENTIFICATION AND QUANTITATIVE EVALUATION

On the basis of the aforementioned parameter setting, the land cover detection map for each dataset can be obtained through the different existing methods and the proposed K-means_AMV separately. To further evaluate the effectiveness of the proposed approach quantitatively, three measurements, namely, false alarm (FA), missed alarm (MA), and total error (TE), are used for experimental comparisons; these measurements have been extensively used in many types of literatures [22], [23], [52], [63], [64]. To clarify the meaning of each measurement, we defined UC as the number of changed pixels that are actually unchanged pixels in the BCDM when compared with the ground reference; TRU is the number of pixels that are unchanged in the ground reference; CU is the number of unchanged pixels in the BCDM but is changed in the ground reference; TRC is the total number of changed pixels in the ground reference truth. Based on these definitions, FA, MA, and TE can be defined as $\frac{UC}{TRU} \times 100\%$, $\frac{CU}{TRC} \times 100\%$ and $\frac{UC+CU}{TRC+TRU} \times 100\%$, correspondingly. In terms of visual identification and quantitative comparisons, the details of the experimental results are presented as follows.

TABLE 3. Comparison between the other methods and the proposed approach for the Lantau Island dataset.

Method	FA(%)	MA(%)	TE(%)
LSELUC	4.53	**4.03**	4.51
MLS	9.4	6.85	9.3
PCA_Kmeans	4.76	4.2	4.73
The proposed-Diff	**1.85**	9.19	**2.2**
The proposed-ARMD	**1.73**	9.37	**2.1**

For the landslide dataset of Hong Kong, China, visual comparison is illustrated in Fig. 5. From these comparisons, the proposed K-means_AMV with an image difference or -ARMD, CMI generation methods clearly performs better than the existing PCA_Kmeans [25], LSELUC [52], and MLS [53] LCCD methods. The proposed approach performs better with less noise than the ground reference map. Furthermore, the shape and size of the landslide area are obtained more accurately than that of other methods in terms of visual identification. The quantitative comparison in Table 3 further strengthens the conclusion of visual identification, in which "the proposed-Diff" and "the proposed-ARMD" presented the proposed approach coupled with the image difference and ARMD CMI generation, respectively. The proposed approaches achieve the optimal detection accuracies in terms of FA and TE in comparison with the PCA_Kmeans [25], LSELUC [52], and MLS [53], as summarized in Table 3.

In the second experiment, two QuickBird satellite images that depict the land use event in the urban Ji Nan City were adopted for experimental comparisons, as demonstrated in Fig. 3. The results of the different methods are exhibited in Fig. 6. From these comparisons, the proposed approaches achieve a better performance with less noise

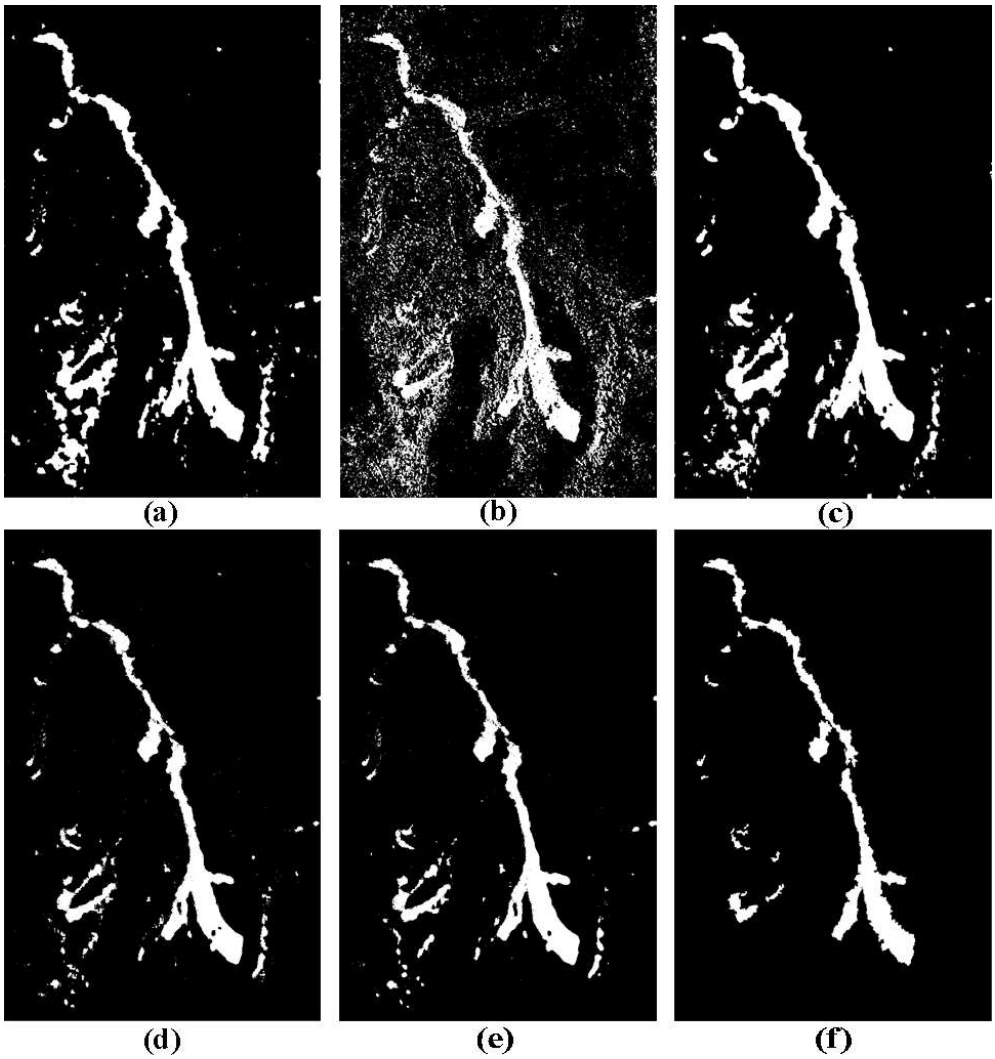

FIGURE 5. Landslide inventory map obtained through the different methods: (a) LSELUC; (b) MLS; (c) PCA-Kmeans; (d) the proposed-Diff; (e) the proposed-ARMD; (f) ground reference map.

TABLE 4. Comparison between the other methods and the proposed approach for the Ji Nan dataset.

Method	FA(%)	MA(%)	TE(%)
LSELUC	10.9	4.15	9.79
MLS	9.75	5.1	8.97
PCA_Kmeans	11	4.6	9.95
The proposed-Diff	9.87	**3.96**	**8.87**
The proposed-ARMD	**9.44**	**4.1**	**8.54**

TABLE 5. Comparison between the other methods and the proposed approach for the Sardinia.

Method	FA(%)	MA(%)	TE(%)
LSELUC	1.42	10.1	1.96
MLS	2.4	**8.56**	2.78
PCA_Kmeans	1.15	12.2	1.83
The proposed-Diff	**0.867**	13.1	**1.62**
The proposed-ARMD	**1.03**	11.8	**1.69**

than the PCA_Kmeans [25], LSELUC [52], and MLS [53]. The quantitative comparisons presented in Table 4 further strengthens the conclusion of the visual comparison and clearly demonstrates that the results obtained through the proposed approaches provide the optimal accuracies in terms of FA, MA, and TE.

To further investigate the generality and performance of the proposed approach, we also apply the proposed approaches to detect a land cover change in an area called Lake Mulargia on Sardinia Island using a remote sensing image. For visual observation, the results obtained through different methods are displayed in Fig. 7. Quantitative comparisons showed that the proposed approaches achieve the optimal accuracies for the Sardinia dataset when compared with the other methods, as listed in Table 5. In addition, the same conclusion can be drawn by the visual performance comparison, as illustrated in Fig. 7. The proposed approach provides the BCDM with a minimal noise and has a close approximation to the ground reference map.

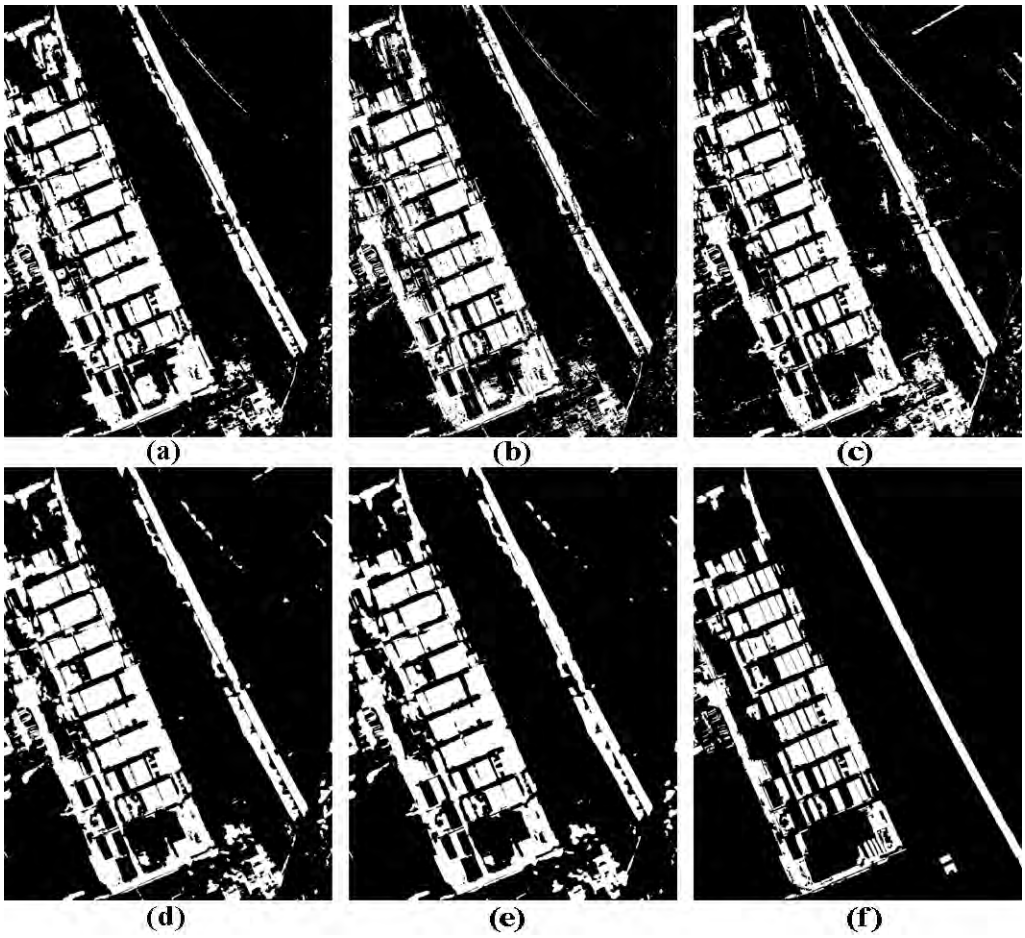

FIGURE 6. Binary LCCD map obtained by the different methods: (a) LSELUC; (b) MLS; (c) PCA-Kmeans; (d) the proposed-Diff; (e) the proposed-ARMD; (f) ground reference map.

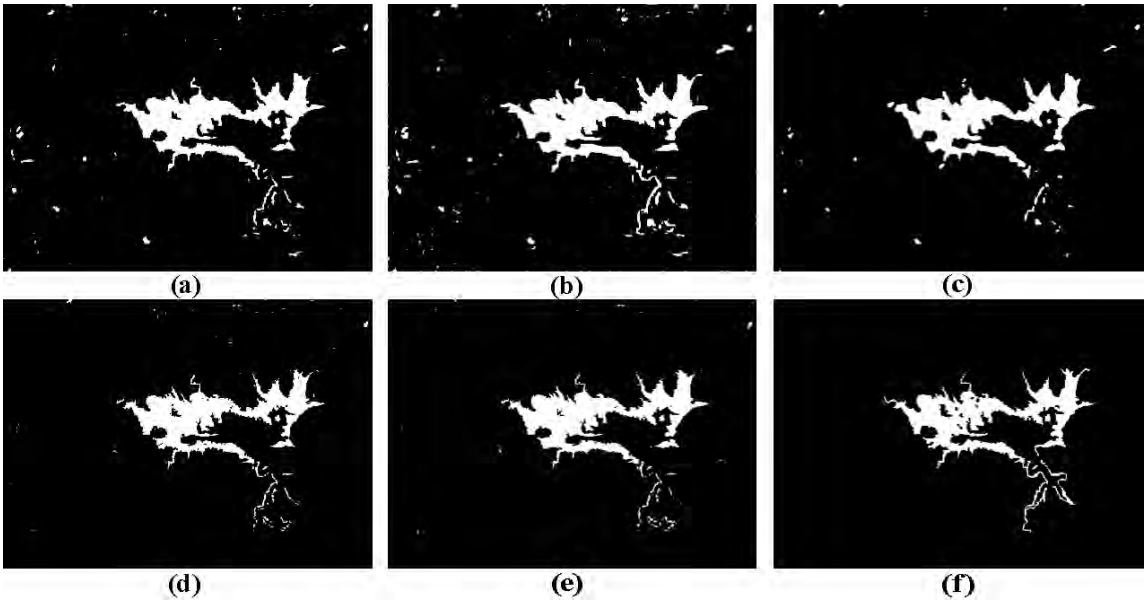

FIGURE 7. Binary LCCD maps obtained through the different methods: (a) LSELUC; (b) MLS; (c) PCA-Kmeans; (d) the proposed-Diff; (e) the proposed-ARMD; (f) ground reference map.

From the visual identifications and quantitative comparisons, the experimental results based on different similar methods, namely, PCA_Kmeans [25], LSELUC [52], and MLS [53], and the proposed approaches, clearly demonstrate

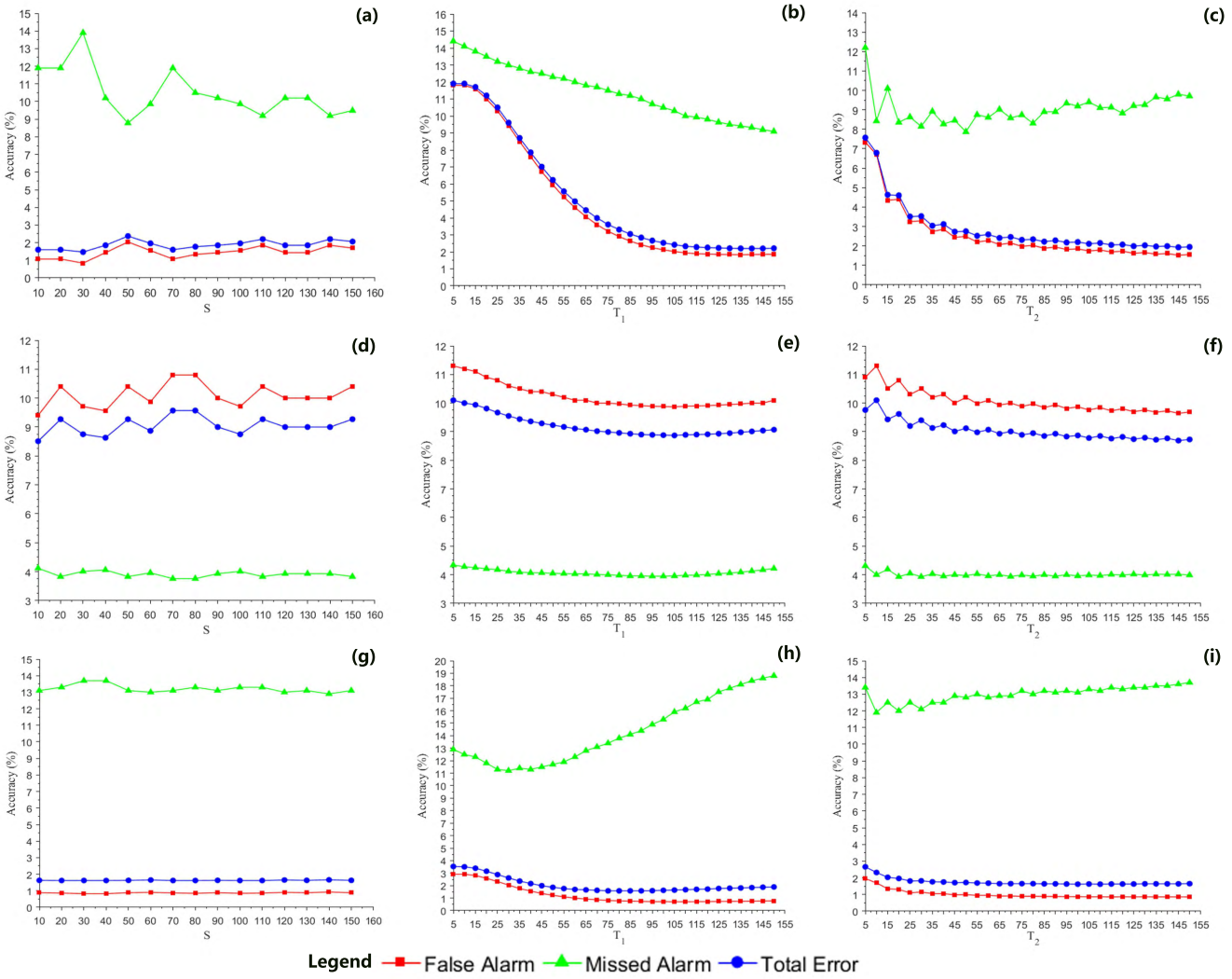

FIGURE 8. Relationship between detection accuracy and parameter setting (S, T_1, and T_2) for the proposed approach with an image difference change magnitude generation in each experiment: (a, b, c) present the relationship between detection accuracies and S, T_1, and T_2 for the Landslide dataset; (d, e, f) display the relationship between detection accuracies and S, T_1, and T_2 for the Ji Nan dataset; (g, h, i) provide the relationship between detection accuracies and S, T_1, and T_2 for the Sardinia dataset.

that the proposed approaches can provide the accurate land cover change map for each land cover change case. Furthermore, the proposed approaches achieve robustness and generality to the remote sensing images from different sourcing platforms with median-low and VHR spatial resolution, including the Landsat-5 satellite images, QuickBird satellite, and aerial photography.

IV. DISCUSSION

From the aforementioned comparisons based on remote sensing images, the proposed approach is more competitive than the PCA_Kmeans [25], LSELUC [52], and MLS [53] in terms of detection accuracies and performance. To promote the application of the proposed approach in practice, the parameter sensitivity of the proposed approach is discussed as follows.

The proposed approach relates to three parameters, namely, sample number (S), T_1, and T_2. Thus, in the discussion, the sensitivity between a parameter and the detection accuracies is analyzed by fixing the value of the two other parameters of the proposed approach, as summarized in Table 6. The relationship between the parameters and detection accuracies for each dataset is depicted in Fig. 8, and the details of the discussion are presented as follows.

TABLE 6. Parameter setting to test the parameter sensitivity for each dataset.

Dataset	S	T_1	T_2
Hong Kong	$T_1 = 145, T_2 = 100$	$S = 100, T_2 = 100$	$S = 100, T_1 = 145$
Ji Nan	$T_1 = 105, T_2 = 100$	$S = 100, T_2 = 100$	$S = 100, T_1 = 105$
Sardian	$T_1 = 70, T_2 = 100$	$S = 100, T_2 = 100$	$S = 100, T_1 = 70$

First, we discuss the sensitivity between S and the detection accuracies. In Figs. 8(a), 8(d), and 8(g), the detection accuracies are fluctuating up and down with the increase in S, whereas the other parameters (T_1 and T_2) are fixed.

Furthermore, the fluctuating degree becomes apparent with the increase in spatial resolution of the remote sensing image because the standard deviation is typically larger in "intra-class" for high spatial resolution remote sensing images than in low spatial resolution remote sensing images [65]. A large standard deviation of intra-class indicates a significant uncertainty of pixels, which consist of a ground target in a remote sensing image. Therefore, the fluctuating degree is varied with the spatial resolution of remote sensing images. In addition, despite the detection accuracies being affected by the sample number, the accuracies will neither increase nor decrease constantly with the increment in S for the three real land cover change cases.

Second, when the value of S and T_2 is fixed, the sensitivity between T_1 and detection accuracies for each dataset is exhibited in Figs. 8(b), 8(e), and 8(h). From this observation, FA and TE initially decrease with the increase in T_1, and they pose gradually to the horizontal level because an increasing spatial information can be utilized with the increment in T_1. However, a very large T_1 may result in additional heterogeneous pixels embraced in an adaptive region, which is detrimental to identifying the label of each pixel using K-means. In addition, in terms of MA, the sensitivity trend varies in different datasets. For example, the MA decreases with the increase in T_1 for the landslide dataset in Hong Kong, the MA nearly maintains a horizontal level with the increase in T_1 for the Ji Nan dataset, and the MA decreases initially and then increases gradually with T_1 for the Sardinian dataset, as displayed in Figs. 8(b), 8(e), and 8(h), correspondingly. When the value of T_1 and S are fixed, the relationship between T_2 and the change detection accuracies is illustrated in Fig. 8. A similar conclusion can be drawn from the relationship between T_1 and the detection accuracies.

From the previous discussion, the following conclusion can be drawn: (1) the first parameter S affects the detection accuracies; however, a large S does not mean a high detection accuracy, especially for the medial-low spatial resolution remote sensing images; (2) T_1 presents the spectral difference between the central pixel and its neighboring pixels, and T_2 constrains the size of an extension; the effect between the parameters and the detection accuracy is different considering the various remote sensing images. Overall, T_1 and T_2 are complementary to each other and must be determined and adjusted in accordance with the different datasets in practical application.

V. CONCLUSION

In this study, a simple but effective LCCD approach has been developed. First, a CMI is prepared on the basis of bitemporal images, and contextual information around a pixel of CMI is utilized through an adaptive region; the pixel is defined as the central pixel of the adaptive region. Then, the pixels within the extended adaptive region are labeled through the classical K-means algorithm pixel-by-pixel. Finally, to further improve the performance of LCCD, the label of the central pixel is refined by the majority voting strategy considering each label of the pixel within the adaptive extended region. Each pixel of the CMI will become the central pixel once, and the final BCDM is generated in this manner. The main contribution of the proposed approach can be summarized briefly as providing a comprehensive fusion of K-means and the majority voting approach for an accurate LCCD using bitemporal remote sensing images. Furthermore, the proposed approach achieves its superiority and robustness over several extensively used methods for the high, median-low spatial resolution remote sensing images.

The proposed approach has been tested using three real land cover change cases using bitemporal remote sensing images. The detection results have been compared quantitatively with PCA_Kmeans [25], LSELUC [52], and MLS [53] on the basis of the same ground reference map. The proposed approach is the most competitive, thereby achieving the highest accuracies in terms of FA, MA, and TE. From the perspective of methodology and practical application, in comparison with PCA_Kmeans [25], LSELUC [52], and MLS [53], the proposed approach has the following advantages:

1) The proposed approach provides competitive change detection results. For the three image scenes that are related to three real land cover change events, the detection results clearly demonstrate the effectiveness and superiority of the proposed approach in terms of visual performance and quantitative accuracies when compared with the similar and widely used methods, namely, PCA_Kmeans [25], LSELUC [52], and MLS [53].
2) To the best of our knowledge, this study is the first to integrate the K-means and the majority voting strategy for LCCD through an adaptive region. The experimental results verify that this comprehensive integration is helpful in improving the detection accuracies and performance because the spatial information utilized in an adaptive manner is more intuitive and objective than that of a regular block for different detection targets with various shapes and sizes.
3) The proposed approach has a high generality. From the experiments, the proposed approach can be applied to different land cover change events, such as landslide inventory mapping and land-use change. Furthermore, the proposed approach achieves robustness to the bitemporal images, which vary in spatial resolution and acquiring platform. Therefore, the proposed approach is relative more than that of PCA_Kmeans [25], LSELUC [52], and MLS [53] general, for practical applications.

In summary, the proposed approach still has limitations despite its advantages and superiority over the extensively used LCCD methods, such as PCA_Kmeans [25], LSELUC [52], and MLS [53], for the real land cover change events based on the bitemporal images with varying spatial resolution. For example, although a binary threshold for obtaining BCDM can be avoided in the proposed approach, the training sample for the changed and unchanged areas must

be initially selected manually before applying our proposed approach. Furthermore, determining the T_1 and T_2 in the proposed approach requires parameter tuning for optimization. Therefore, in the future study, the automation parameters of the proposed approach will be considered.

ACKNOWLEDGMENT

The authors thank the editor-in-chief, associate editor, and reviewers for their insightful comments and suggestions.

REFERENCES

[1] A. Singh, "Review article digital change detection techniques using remotely-sensed data," *Int. J. Remote Sens.*, vol. 10, no. 6, pp. 989–1003, 1989.

[2] V. Walter, "Object-based classification of remote sensing data for change detection," *ISPRS J. Photogramm. Remote Sens.*, vol. 58, nos. 3–4, pp. 225–238, 2004.

[3] D. Lu, P. Mausel, E. Brondízio, and E. Moran, "Change detection techniques," *Int. J. Remote Sens.*, vol. 25, no. 12, pp. 2365–2401, 2004.

[4] H. Nemmour and Y. Chibani, "Multiple support vector machines for land cover change detection: An application for mapping urban extensions," *I SPRS J. Photogram. Remote Sens.*, vol. 61, no. 2, pp. 125–133, 2006.

[5] J. Xiao *et al.*, "Evaluating urban expansion and land use change in Shijiazhuang, China, by using GIS and remote sensing," *Landscape Urban Planning*, vol. 75, nos. 1–2, pp. 69–80, Feb. 2006.

[6] Q. Zhang, J. Wang, X. Peng, P. Gong, and P. Shi, "Urban built-up land change detection with road density and spectral information from multi-temporal Landsat TM data," *Int. J. Remote Sens.*, vol. 23, no. 15, pp. 3057–3078, Jan. 2002.

[7] X. Huang, L. Zhang, and T. Zhu, "Building change detection from multitemporal high-resolution remotely sensed images based on a morphological building index," *IEEE J. Sel. Topics Appl. Earth Observat. Remote Sens.*, vol. 7, no. 1, pp. 105–115, Jan. 2014.

[8] Q. Weng, D. Lu, and J. Schubring, "Estimation of land surface temperature-vegetation abundance relationship for urban heat island studies," *Remote Sens. Environ.*, vol. 89, no. 4, pp. 467–483, Feb. 2004.

[9] Z. Li, W. Shi, P. Lu, L. Yan, Q. Wang, and Z. Miao, "Landslide mapping from aerial photographs using change detection-based Markov random field," *Remote Sens. Environ.*, vol. 187, pp. 76–90, Dec. 2016.

[10] Z. Li, W. Shi, S. W. Myint, P. Lu, and Q. Wang, "Semi-automated landslide inventory mapping from bitemporal aerial photographs using change detection and level set method," *Remote Sens. Environ.*, vol. 175, pp. 215–230, Mar. 2016.

[11] J. Nichol and M. Wong, "Satellite remote sensing for detailed landslide inventories using change detection and image fusion," *Int. J. Remote Sens.*, vol. 26, no. 9, pp. 1913–1926, May 2005.

[12] T. Hermosilla, M. A. Wulder, J. C. White, N. C. Coops, and G. W. Hobart, "Regional detection, characterization, and attribution of annual forest change from 1984 to 2012 using Landsat-derived time-series metrics," *Remote Sens. Environ.*, vol. 170, pp. 121–132, Dec. 2015.

[13] P. V. Potapov *et al.*, "Eastern Europe's forest cover dynamics from 1985 to 2012 quantified from the full Landsat archive," *Remote Sens. Environ.*, vol. 159, pp. 28–43, Mar. 2015.

[14] J. O. Sexton *et al.*, "A model for the propagation of uncertainty from continuous estimates of tree cover to categorical forest cover and change," *Remote Sens. Environ.*, vol. 156, pp. 418–425, Jan. 2015.

[15] J. Yang, M. S. Wong, M. Menenti, and J. Nichol, "Study of the geometry effect on land surface temperature retrieval in urban environment," *ISPRS J. Photogram. Remote Sens.*, vol. 109, pp. 77–87, Nov. 2015.

[16] M. K. Ridd and J. Liu, "A comparison of four algorithms for change detection in an urban environment," *Remote Sens. Environ.*, vol. 63, no. 2, pp. 95–100, 1998.

[17] P. Coppin, I. Jonckheere, K. Nackaerts, B. Muys, and E. Lambin, "Review articledigital change detection methods in ecosystem monitoring: A review," *Int. J. Remote Sens.*, vol. 25, no. 9, pp. 1565–1596, 2004.

[18] L. Yang, G. Xian, J. M. Klaver, and B. Deal, "Urban land-cover change detection through sub-pixel imperviousness mapping using remotely sensed data," *Photogramm. Eng. Remote Sens.*, vol. 69, no. 9, pp. 1003–1010, Sep. 2003.

[19] O. A. El-Kawy, J. Rød, H. Ismail, and A. Suliman, "Land use and land cover change detection in the western Nile delta of Egypt using remote sensing data," *Appl. Geography*, vol. 31, no. 2, pp. 483–494, Apr. 2011.

[20] Z. Lv and W. Zhang, "Contextual analysis based approach for detecting change from high resolution satellite imagery," *J. Indian Soc. Remote Sens.*, vol. 46, no. 1, pp. 43–50, Jan. 2018.

[21] Z. Lv, W. Z. Shi, X. Zhou, and J. A. Benediktsson, "Semi-automatic system for land cover change detection using bi-temporal remote sensing images," *Remote Sens.*, vol. 9, no. 11, p. 1112, Oct. 2017.

[22] L. Bruzzone and D. F. Prieto, "Automatic analysis of the difference image for unsupervised change detection," *IEEE Trans. Geosci. Remote Sens.*, vol. 38, no. 3, pp. 1171–1182, May 2000.

[23] L. Bruzzone and D. F. Prieto, "An adaptive semiparametric and context-based approach to unsupervised change detection in multitemporal remote-sensing images," *IEEE Trans. Image Process.*, vol. 11, no. 4, pp. 452–466, Apr. 2002.

[24] R. J. Radke, S. Andra, O. Al-Kofahi, and B. Roysam, "Image change detection algorithms: A systematic survey," *IEEE Trans. Image Process.*, vol. 14, no. 3, pp. 294–307, Mar. 2005.

[25] T. Celik, "Unsupervised change detection in satellite images using principal component analysis and *k*-means clustering," *IEEE Geosci. Remote Sens. Lett.*, vol. 6, no. 4, pp. 772–776, Oct. 2009.

[26] F. Bovolo and L. Bruzzone, "A theoretical framework for unsupervised change detection based on change vector analysis in the polar domain," *IEEE Trans. Geosci. Remote Sens.*, vol. 45, no. 1, pp. 218–236, Jan. 2007.

[27] H. Zhuang, K. Deng, H. Fan, and M. Yu, "Strategies combining spectral angle mapper and change vector analysis to unsupervised change detection in multispectral images," *IEEE Geosci. Remote Sens. Lett.*, vol. 13, no. 5, pp. 681–685, May 2016.

[28] J. Chen, M. Lu, X. Chen, J. Chen, and L. Chen, "A spectral gradient difference based approach for land cover change detection," *ISPRS J. Photogram. Remote Sens.*, vol. 85, pp. 1–12, Nov. 2013.

[29] N. Otsu, "A threshold selection method from gray-level histograms," *IEEE Trans. Syst., Man, Cybern.*, vol. 9, no. 1, pp. 62–66, Jan. 1979.

[30] M. Hao, W. Shi, H. Zhang, and C. Li, "Unsupervised change detection with expectation-maximization-based level set," *IEEE Geosci. Remote Sens. Lett.*, vol. 11, no. 1, pp. 210–214, Jan. 2014.

[31] J. Chen, P. Gong, C. He, R. Pu, and P. Shi, "Land-use/land-cover change detection using improved change-vector analysis," *Photogramm. Eng. Remote Sens.*, vol. 69, no. 4, pp. 369–379, 2003.

[32] M. C. Hansen and T. R. Loveland, "A review of large area monitoring of land cover change using Landsat data," *Remote Sens. Environ.*, vol. 122, pp. 66–74, Jul. 2012.

[33] R. S. Lunetta, J. F. Knight, J. Ediriwickrema, J. G. Lyon, and L. D. Worthy, "Land-cover change detection using multi-temporal MODIS NDVI data," *Remote Sens. Environ.*, vol. 105, no. 2, pp. 142–154, 2006.

[34] S. Jin, L. Yang, P. Danielson, C. Homer, J. Fry, and G. Xian, "A comprehensive change detection method for updating the national land cover database to circa 2011," *Remote Sens. Environ.*, vol. 132, pp. 159–175, May 2013.

[35] X. Zhan *et al.*, "Detection of land cover changes using MODIS 250 m data," *Remote Sens. Environ.*, vol. 83, nos. 1–2, pp. 336–350, Nov. 2002.

[36] I. Klein, U. Gessner, and C. Kuenzer, "Regional land cover mapping and change detection in central asia using MODIS time-series," *Appl. Geography*, vol. 35, nos. 1–2, pp. 219–234, Nov. 2012.

[37] S. Muster, M. Langer, A. Abnizova, K. L. Young, and J. Boike, "Spatio-temporal sensitivity of MODIS land surface temperature anomalies indicates high potential for large-scale land cover change detection in Arctic permafrost landscapes," *Remote Sens. Environ.*, vol. 168, pp. 1–12, Oct. 2015.

[38] Z. Zhu and C. E. Woodcock, "Continuous change detection and classification of land cover using all available landsat data," *Remote Sens. Environ.*, vol. 144, pp. 152–171, Mar. 2014.

[39] C. Homer *et al.*, "Completion of the 2011 National Land Cover Database for the conterminous United States-representing a decade of land cover change information," *Photogramm. Eng. Remote Sens.*, vol. 81, no. 5, pp. 345–354, May 2015.

[40] Z. Zhu *et al.*, "Including land cover change in analysis of greenness trends using all available Landsat 5, 7, and 8 images: A case study from Guangzhou, China (2000–2014)," *Remote Sens. Environ.*, vol. 185, pp. 243–257, Nov. 2016.

[41] M. Hornacek *et al.*, "Potential for high resolution systematic global surface soil moisture retrieval via change detection using Sentinel-1," *IEEE J. Sel. Topics Appl. Earth Observ. Remote Sens.*, vol. 5, no. 4, pp. 1303–1311, Aug. 2012.
[42] Z. Zhu, S. Wang, and C. E. Woodcock, "Improvement and expansion of the Fmask algorithm: Cloud, cloud shadow, and snow detection for Landsats 4–7, 8, and Sentinel 2 images," *Remote Sens. Environ.*, vol. 159, pp. 269–277, Mar. 2015.
[43] J. Muro *et al.*, "Short-term change detection in wetlands using sentinel-1 time series," *Remote Sens.*, vol. 8, no. 10, p. 795, Sep. 2016.
[44] F. Luo, H. Huang, Y. Duan, J. Liu, and Y. Liao, "Local geometric structure feature for dimensionality reduction of hyperspectral imagery," *Remote Sens.*, vol. 9, no. 8, p. 790, Aug. 2017.
[45] F. Luo *et al.*, "Feature learning using spatial-spectral hypergraph discriminant analysis for hyperspectral image," *IEEE Trans. Cybern.*, to be published.
[46] L. Bruzzone and F. Bovolo, "A novel framework for the design of change-detection systems for very-high-resolution remote sensing images," *Proc. IEEE*, vol. 101, no. 3, pp. 609–630, Mar. 2013.
[47] Y. Du, P. M. Teillet, and J. Cihlar, "Radiometric normalization of multitemporal high-resolution satellite images with quality control for land cover change detection," *Remote Sens. Environ.*, vol. 82, no. 1, pp. 123–134, Sep. 2002.
[48] Y. Byun, Y. Han, and T. Chae, "Image fusion-based change detection for flood extent extraction using bi-temporal very high-resolution satellite images," *Remote Sens.*, vol. 7, no. 8, pp. 10347–10363, Aug. 2015.
[49] T. Blaschke, "Object based image analysis for remote sensing," *ISPRS J. Photogram. Remote Sens.*, vol. 65, no. 1, pp. 2–16, Jan. 2010.
[50] M. Hussain, D. Chen, A. Cheng, H. Wei, and D. Stanley, "Change detection from remotely sensed images: From pixel-based to object-based approaches," *ISPRS J. Photogramm. Remote Sens.*, vol. 80, pp. 91–106, Jun. 2013.
[51] W. Zhou, A. Troy, and M. Grove, "Object-based land cover classification and change analysis in the baltimore metropolitan area using multitemporal high resolution remote sensing data," *Sensors*, vol. 8, no. 3, pp. 1613–1636, Mar. 2008.
[52] X. Zhang, W. Shi, P. Liang, and M. Hao, "Level set evolution with local uncertainty constraints for unsupervised change detection," *Remote Sens. Lett.*, vol. 8, no. 8, pp. 811–820, May 2017.
[53] Y. Bazi, F. Melgani, and H. D. Al-Sharari, "Unsupervised change detection in multispectral remotely sensed imagery with level set methods," *IEEE Trans. Geosci. Remote Sens.*, vol. 48, no. 8, pp. 3178–3187, Aug. 2010.
[54] G. Cui *et al.*, "Refining land cover classification maps based on dual-adaptive majority voting strategy for very high resolution remote sensing images," *Remote Sens.*, vol. 10, no. 8, p. 1238, 2018.
[55] L. ZhiYong, W. Shi, J. A. Benediktsson, and L. Gao, "A modified mean filter for improving the classification performance of very high-resolution remote-sensing imagery," *Int. J. Remote Sens.*, vol. 39, no. 3, pp. 770–785, 2018.
[56] T. Lei, X. Jia, and Y. Zhang, "Superpixel-based fast fuzzy C-means clustering for color image segmentation," *IEEE Trans. Fuzzy Syst.*, to be published.
[57] L. Fang, S. Li, X. Kang, and J. A. Benediktsson, "Spectral-spatial hyperspectral image classification via multiscale adaptive sparse representation," *IEEE Trans. Geosci. Remote Sens.*, vol. 52, no. 12, pp. 7738–7749, Dec. 2014.
[58] M. Xiong, Q. Ran, W. Li, J. Zou, and Q. Du, "Hyperspectral image classification using weighted joint collaborative representation," *IEEE Geosci. Remote Sens. Lett.*, vol. 12, no. 6, pp. 1209–1213, Jun. 2015.
[59] W. R. Tobler, "A computer movie simulating urban growth in the Detroit region," *Econ. Geogr.*, vol. 46, pp. 234–240, Jun. 1970.
[60] X. Jing, S. Y. Chen, and L. L. Fan, "Semi-supervised classification of multi-spectral images based on density: Selected samples," in *Proc. 9th Int. Conf. Digit. Image Process. (ICDIP), Int. Soc. Opt. Photon.*, Hong Kong, vol. 10420, 2017, Art. no. 1042030.
[61] Z. Lv, T. Liu, Y. Wan, J. A. Benediktsson, and X. Zhang, "Post-processing approach for refining raw land cover change detection of very high-resolution remote sensing images," *Remote Sens.*, vol. 10, no. 3, p. 472, 2018.
[62] Z. Lv, T. Liu, P. Zhang, J. A. Benediktsson, and Y. Chen, "Land Cover Change Detection Based on Adaptive 2 Contextual Information Using Bi-Temporal Remote Sensing Images," *Remote Sens.*, no. 10, p. 901, May 2018.
[63] A. Ghosh, N. S. Mishra, and S. Ghosh, "Fuzzy clustering algorithms for unsupervised change detection in remote sensing images," *Inf. Sci.*, vol. 181, no. 4, pp. 699–715, 2011.
[64] Z. Yetgin, "Unsupervised change detection of satellite images using local gradual descent," *IEEE Trans. Geosci. Remote Sens.*, vol. 50, no. 5, pp. 1919–1929, May 2012.
[65] L. Zhang, X. Huang, B. Huang, and P. Li, "A pixel shape index coupled with spectral information for classification of high spatial resolution remotely sensed imagery," *IEEE Trans. Geosci. Remote Sens.*, vol. 44, no. 10, pp. 2950–2961, Oct. 2006.

ZHIYONG LV received the M.S. and Ph.D. degrees from the School of Remote Sensing and Information Engineering, Wuhan University, Wuhan, China, in 2008 and 2014, respectively. He was an Engineer of surveying with the First Institute of Photogrammetry and Remote Sensing, from 2008 to 2011. He is currently with the School of Computer Science and Engineering, Xi'an University of Technology. His research interests include multi hyperspectral and high-resolution remotely sensed image processing, spatial feature extraction, neural networks, pattern recognition, deep learning, and remote sensing applications.

TONGFEI LIU is currently pursuing the master's degree in computer science with the Xi'an University of Technology, China. He is interested in spatial–spectral feature extraction, pattern recognition, ground target detection, and land cover/land use change detection, through remote sensing image with high or very high spatial resolution (including satellite imagery and aerial images).

CHENG SHI received the B.S. degree from the Xi'an University of Architecture and Technology, China, in 2009, and the M.S. and Ph.D. degrees from Xidian University, China, in 2012 and 2016, respectively. In 2018, she joined the University of Macau, China, as a Postdoctoral Research Fellow. She is currently with the School of Computer Science and Engineering, Xi'an University of Technology. Her research interests include deep learning, image processing, and pattern recognition.

JÓN ATLI BENEDIKTSSON received the Cand.Sci. degree in electrical engineering from the University of Iceland, Reykjavik, in 1984, and the M.S.E.E. and Ph.D. degrees from Purdue University, West Lafayette, IN, in 1987 and 1990, respectively. He is currently a Pro Rector for academic affairs and a Professor of electrical and computer engineering with the University of Iceland. He is a Co-Founder of the biomedical startup company, Oxymap. His research interests include remote sensing, biomedical analysis of signals, pattern recognition, image processing, and signal processing. He has published extensively in the above-mentioned fields. He is a Fellow of SPIE. He is a member of the Association of Chartered Engineers in Iceland (VFI), Societas Scientiarum Islandica, and Tau Beta Pi. He received the Stevan J. Kristof Award from Purdue University, in 1991, as an outstanding graduate student in remote sensing. He was a recipient of the Icelandic Research Council's Outstanding Young Researcher Award, in 1997, the IEEE Third Millennium Medal, in 2000, and the IEEE/VFI Electrical Engineer of the Year Award, in 2013. He was a co-recipient of the University of Iceland's Technology Innovation Award, in 2004, the 2012 IEEE Transactions on Geoscience and Remote Sensing Paper Award, and the IEEE GRSS Highest Impact Paper Award, in 2013. He received the Yearly Research Award from the Engineering Research Institute, University of Iceland, in 2006, and the Outstanding Service Award from the IEEE Geoscience and Remote Sensing Society, in 2007. He was the President of the IEEE Geoscience and Remote Sensing Society (GRSS), from 2011 to 2012. He has been with the GRSS AdCom, since 2000. He was the Editor of the IEEE TRANSACTIONS ON GEOSCIENCE AND REMOTE SENSING (TGRS), from 2003 to 2008. He has been serving as an Associate Editor for TGRS, since 1999, IEEE GEOSCIENCE AND REMOTE SENSING LETTERS, since 2003, and the IEEE ACCESS, since 2013. He is on the International Editorial Board of the *International Journal of Image and Data Fusion*. He was the Chairman of the Steering Committee of the IEEE JOURNAL OF SELECTED TOPICS IN APPLIED EARTH OBSERVATIONS AND REMOTE SENSING (J-STARS), from 2007 to 2010.

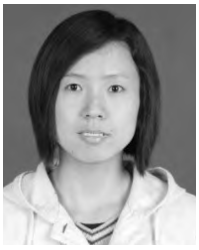

HEJUAN DU was born in 1982. She received the M.S. degree from Nanjing University, in 2008, and the Ph.D. degree from the Institute of Digital Earth and Remote Sensing, Chinese Academy of Sciences, in 2013. She majored in jointly modeling and vegetation LAI retrieval by optical and microwave remote sensing. She has published more than five research papers in her research fields.